ELSEVIER

Composites: Part A 33 (2002) 1055–1062

composites
Part A: applied science and manufacturing

www.elsevier.com/locate/compositesa

Low-velocity impact-induced damage of continuous fiber-reinforced composite laminates. Part I. An FEM numerical model

C.F. Li[a,*], N. Hu[b], Y.J. Yin[a], H. Sekine[c], H. Fukunaga[c]

[a]*Department of Engineering Mechanics, Tsinghua University, Beijing 100084, People's Republic of China*
[b]*Department of Mechanical Engineering, The Johns Hopkins University, 3400 N. Charles Street, Baltimore, MD 21218, USA*
[c]*Department of Aeronautics and Space Engineering, Tohoku University, 01 Aramaki-aoba, Aoba-ku, Sendai 980-8579, Japan*

Received 21 September 2001; revised 14 June 2002; accepted 26 June 2002

Abstract

A numerical model for simulating the process of low-velocity impact damage in composite laminates using the finite element method is presented in this paper, i.e. Part I of this two part series on the study of impact. In this model, the 9-node Lagrangian element of the Mindlin plate with consideration of large deformation analysis is employed. To analyze the transient response of the laminated plates, a modified Newmark time integration algorithm previously proposed by the authors is adopted here. We also proved that the impact process between a rigid ball and laminated plates is a stiff system, therefore a kind of $A(\alpha)$ stable method has been advocated here to solve the motion equation of the rigid ball. Furthermore, various types of damages including delamination, matrix cracking and fiber breakage, etc. and their mutual influences are modeled and investigated in detail. To overcome the difficulty of numerical oscillation or instability in the analysis of the dynamic contact problem between delaminated layers using the traditional penalty methods, we have employed dynamic spring constraints to simulate the contact effect, which are added to the numerical model by a kind of continuous penalty function. Moreover, an effective technique to calculate the strain energy release rate based on the Mindlin plate model is proposed, which can attain high precision. Finally, some techniques of adaptive analyses have been realized for improving the computational efficiency. Based on this model, a program has been developed for numerically simulating the damage process of cross-ply fiber-reinforced carbon/epoxy composite laminates under low-velocity impact load. In Part II, this numerical model will be verified by comparing with the experimental results. Also the impact damage will be investigated in detail using this numerical approach.

Keywords: A. Polymer–matrix composites (PMCs); B. Fracture; B. Impact behavior; C. Finite element analysis (FEA)

1. Introduction

It is well known that organic matrix fiber-reinforced composite laminates are very susceptible to low-velocity transverse impact. It has been shown by many researchers that low-velocity transverse impact could cause various damages, such as matrix cracks, delamination and fiber breakage. Such damages are very difficult to be detected by naked eyes and can cause significant reductions in the strength and stiffness of the materials. Hence, it is crucial to understand the mechanisms and mechanics of the impact damage in the laminates.

Till now, extensive investigations have been conducted on this subject. Most of the earlier work concentrated on the experimental investigations. Within recent years, some efficient numerical models have also been set up for studying this problem. For instance, some researchers employed the 2D FEM to study a beam-like model [1–3]. These approaches for analyzing the beam-like model are computationally very efficient due to its simplicity and can be used to study some fundamental problems in this field. However, this numerical model for plane-strain problems may fail to provide more detailed and comprehensive information, such as the in-plane delamination shape in the laminated plates. To perform more detailed stress analyses in the laminates, many authors have studied this problem based on the 3D FEM model [4–6]. However, there are some apparent difficulties in the 3D FEM, such as the exorbitant computational cost and the automatic mesh generation with the extension of delamination. To overcome the difficulties faced in the 3D FEM model, some

* Corresponding author. Tel.: +86-130-01917475; fax: +86-010-62781824.
E-mail address: lichenfeng99@mails.tsinghua.edu.cn (C.F. Li).

1359-835X/02/$ - see front matter
PII: S1359-835X(02)00081-7

researchers employed the 2D plate model to study this problem [7–9]. It can be found that most researches till now have been mainly concentrating on the following several aspects: (1) mechanisms of damage formation, especially the onset of various damages [2,3]; (2) dynamic fracture toughness for delamination extension [1,10]; (3) threshold of impact energy or velocity [3,9]; (4) relationship between damage sizes and the various impact parameters [4,7,10]. Very limited work has been reported about the full and direct numerical simulation of the whole damage process. Actually, most of the present numerical approaches have only roughly evaluated the delamination sizes using some simple empirical formulae [4,6,7] or simplified models with the help of the experimental information [8].

With the previous background in mind, the objective of the present paper is to develop an integrated and elaborate numerical model, which can describe the various damages and their mutual effects. For this purpose, based on our previous work [11–13] we have built up an FEM model based on the Mindlin [14] plate element for directly and completely simulating the low-velocity impact-induced damages in laminated plates. Various aspects in this model, such as the damage criteria, update of plate stiffness, dynamic contact problem between delaminated layers, adaptive analyses, etc. have been studied in detail. Some new and effective techniques have also been put forward for increasing the computational efficiency.

2. Description of damage patterns

For the sake of simplicity, only the cross-ply, i.e. 0°/90°/0° composite plates have been considered here, and Fig. 1 presents several typical damage patterns in the plates induced by low-velocity impact. From this figure, there are at least two main categories of damages that can be identified clearly, i.e. the matrix cracks and the delamination of a peanut shape. There are two kinds of matrix cracks due to tension and shear in this figure, which can be observed very clearly. The first one is a long bending matrix crack along the horizontal or 0° direction whose length is usually the same as or even longer than that of the peanut delamination as shown in Fig. 1. The second one is some short shear matrix cracks near the impact location, which are aligned in the vertical or 90° direction. Another main kind of damages, i.e. the delamination of a peanut shape, can also be identified in Fig. 1. This delamination is located on the bottom interface, i.e. 90°/0° interface, with the peanut shape elongating in the direction of the fibers in the lower ply. Also, there are other two kinds of damages, i.e. the fiber breakage due to tension and the matrix crushing due to compression. Generally, these two kinds of damages patterns are not the principal ones induced by the low-velocity impact. From some previous researches [4,10], the common damage process induced by low-velocity impact loads can be described as follows: the impact load first causes shear matrix cracks in the second 90° layer, which can generate delamination immediately along the bottom or upper interface of the cracked layer. As the impact event proceeds, additional bending matrix cracks can occur subsequently in the third 0° layer and can produce additional delamination along the bottom interface. Usually, the delamination triggered by the shear matrix cracks on the upper interface, i.e. 0°/90° interface, only propagates unstably toward the impact location. Hence, its size is usually very small with negligible consumption of impact energy. On the other hand, the major delamination on the bottom interface as shown in Fig. 1, which is caused by the shear cracks and bending cracks and dominated by the bending cracks, extends very stably. This major delamination of the peanut shape is of particular interest here and will be only considered in the present study.

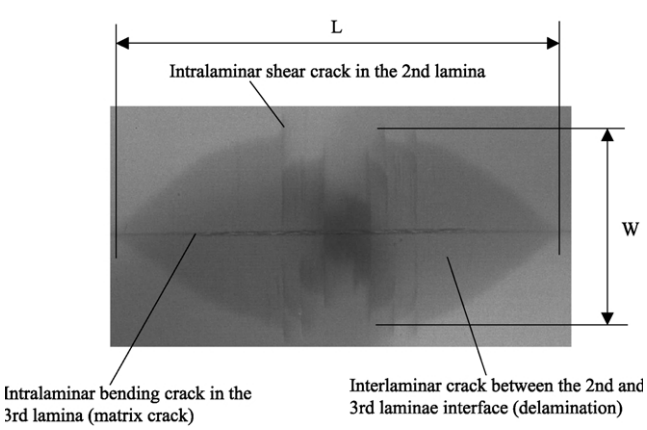

Fig. 1. Damage in cross-ply laminates under low-velocity impact.

3. FEM model and numerical techniques

3.1. Impact dynamics

Due to the low computational cost and strong ability, the Mindlin plate element [14], which takes transverse shear deformation and large deformation into account and has 5 DOFs $(\hat{u}_i, \hat{v}_i, \hat{w}_i, \theta_{xi}, \theta_{yi})^{\mathrm{T}}$ on each node, has been chosen. The system equation for describing the motion of the plates is

$$\mathbf{M}\ddot{\hat{\mathbf{u}}} + \mathbf{K}\hat{\mathbf{u}} = \hat{\mathbf{p}} - \hat{\mathbf{F}} \tag{1}$$

where $\hat{\mathbf{p}}$ is the equivalent external load corresponding to the displacement $\hat{\mathbf{u}}$, which includes the impact force from the rigid ball, and $\hat{\mathbf{F}}$ is the equivalent load corresponding to the non-linear items of strain [14] due to large deformation.

A rigid ball of mass m_s and velocity v impacts transversely at the center of the plates as shown in Fig. 2. The dynamic equation of the rigid ball is

$$m_s\ddot{w}_s = F - m_s g \tag{2}$$

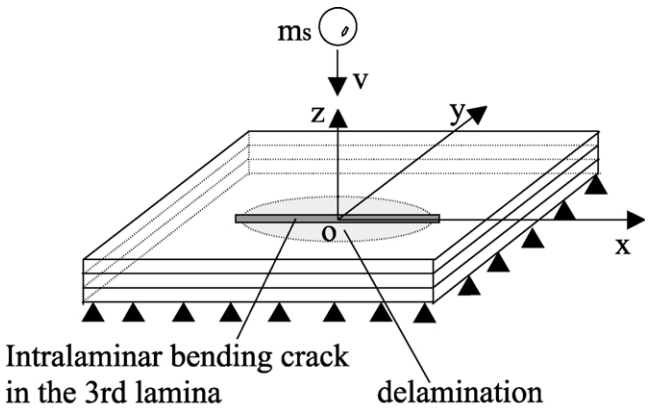

Fig. 2. Impact model.

where m_s is the mass of the rigid ball and F is the impact reaction force.

The impact reaction force connecting the ball and the plates can be calculated using a modified Hertz indentation law proposed by Tan and Sun [15]

$$F = \begin{cases} k\alpha^{1.5} & \text{loading} \\ F_m\left(\dfrac{\alpha-\alpha_0}{\alpha_m-\alpha_0}\right)^q & \text{unloading} \end{cases}, \qquad \alpha_0 = \begin{cases} \beta(\alpha_m-\alpha_{cr}) & (\alpha_m > \alpha_{cr}) \\ 0 & (\alpha_m \le \alpha_{cr}) \end{cases} \tag{3}$$

where k, q, β and α_{cr} are experimental constants, α_m is the maximum of the indentation depth during loading process, F_m is the maximum of the impact force before unloading stage, α_0 is the permanent indentation depth and α is the indentation depth. In order to stabilize the FEM analysis, we apply a uniformly distributed load on the central small element of the laminates, instead of a single concentrated force F [12,13].

Because of the different characteristics of Eqs. (1) and (2), they are solved independently, and are connected using the iteration process for solving Eq. (3). We have adopted a modified Newmark algorithm proposed by authors [11] to solve Eq. (1) for obtaining the stable transient response of plates. We have also found that if the central difference scheme or the Newmark scheme is used for Eq. (2), the time increment must be controlled to be small enough, e.g. $\Delta t < 0.001$, ms, in order to avoid numerical instability or ensure calculation precision. Here, we examined Eq. (2) to uncover the problem, and then proposed an efficient time integration scheme.

Without losing generality, in the loading process, by substituting Eq. (3) into Eq. (2), we can obtain the transient dynamic equation of the rigid ball as:

$$m_s\ddot{w}_s = k(\hat{w}-w_s)^{1.5} - m_s g \Leftrightarrow \begin{cases} \dot{w}_s = v_s \\ \dot{v}_s = \dfrac{1}{m_s}k(\hat{w}-w_s)^{1.5} - g \end{cases} \tag{4}$$

Here, we assume that the displacement of laminates on the impact point $\hat{w} = \text{Const}$. Expanding the above equation into Taylor's series leads to:

$$\begin{cases} \dot{w}_s = v_s \\ \dot{v}_s = -\dfrac{1.5}{m_s}k(\hat{w}-w_0)^{0.5}w_s + \dfrac{1.5}{m_s}k(\hat{w}-w_0)^{0.5}w_0 \\ \qquad\quad + \dfrac{1}{m_s}k(\hat{w}-w_0)^{1.5} - g \end{cases} \tag{5}$$

This linear ordinary differential equation system is found to be a stiff system [16] from its two eigenvalues. Thus we utilize the following $A(\alpha)$ stable fourth-order method proposed by Gear [16] to solve Eq. (2)

$$\mathbf{Y}_{n+4} = \frac{1}{25}(48\mathbf{Y}_{n+3} - 36\mathbf{Y}_{n+2} + 16\mathbf{Y}_{n+1} - 3\mathbf{Y}_n + 12h\mathbf{F}_{n+4}) \tag{6}$$

where $\mathbf{Y} = \{w_s, v_s\}^T$ and $\mathbf{F} = \{v_s, (1/m_s)k(\hat{w}-w_s)^{1.5} - g\}^T$, and h denotes the increment between two immediate time steps.

Numerical experiments have shown that the large time increment can be used to accomplish an impact process in the above scheme.

3.2. Modeling failures of fiber and matrix

Recently, Hou et al. [6] summarized the stress-based failure criteria for fiber failure, matrix cracking and matrix crushing as shown in Fig. 3 and Table 1. This technique is

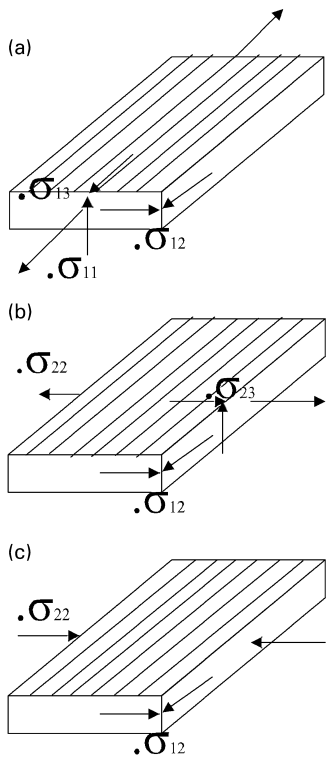

Fig. 3. (a) Fiber failure; (b) matrix cracking; (c) matrix crushing.

Table 1
Failure criteria of fiber and matrix and strategy of updating stresses [8]

Failure stress state	Failure criteria	Updating strategy of stresses
Fiber failure	$\left(\frac{\sigma_{11}}{X_T}\right)^2+\left(\frac{\sigma_{12}^2+\sigma_{13}^2}{S_f^2}\right)\geq 1$	$\sigma_{11}=\sigma_{22}=\sigma_{33}=0,$ $\sigma_{12}=\sigma_{23}=\sigma_{31}=0$
Matrix cracking if $\sigma_{22}\geq 0$	$\left(\frac{\sigma_{22}}{Y_T}\right)^2+\left(\frac{\sigma_{12}}{S_{12}}\right)^2+\left(\frac{\sigma_{23}}{S_{m23}}\right)^2\geq 1$	$\sigma_{22}=0,\ \sigma_{12}=0$
Matrix crushing if $\sigma_{22}<0$	$\frac{1}{4}\left(\frac{-\sigma_{22}}{S_{12}}\right)^2+\frac{Y_C^2\sigma_{22}}{4S_{12}^2Y_C}-\frac{\sigma_{22}}{Y_C}+\left(\frac{\sigma_{12}}{S_{12}}\right)^2\geq 1$	$\sigma_{22}=0$

X_T: fiber directional (1-axis) tensile strength; Y_T: transversal (2-axis) tensile strength; Y_C: transversal (2-axis) compressive strength; S_{12}: laminates' plane (1–2 plane) shearing strength; S_f: shearing strength causing fiber failure; S_{m23}: cross sectional (2–3 plane) shearing strength causing matrix cracking.

obviously based on some average meaning, which has been adopted by many previous studies [4–6,10] to deal with these three types of failure. Here, we adopted this technique [6]. Furthermore, according to Maxwell's principle $v_{ij}/E_j = v_{ji}/E_i$ and the constitutive relation of the single layer in laminates, we introduce a strategy for updating the stresses and the equivalent strategy for updating elastic constants as shown in Table 2.

The failure criteria in Table 1 are used to check the failure state of each layer in every element for laminates. At first, five stress components within a specific layer of an element are obtained by averaging the corresponding components from nine Gaussian points within the element, and then submitted into the failure criteria. If the stress state satisfies the failure criteria, the material constants in this layer of the element should be modified according to the strategy in Table 2. Parameters d and e in Table 2, which are determined by pilot calculation, describe damage-resisting capability of laminates.

3.3. Modeling delamination

Some authors also deal with the delamination using the one-off stress-based failure criteria, e.g. [4,6]. Although it was partially successful in some limited cases, its applicability to predict the delamination damage remains unjustified [10] since the stress field is redistributed at the onset of delamination. Davies and Zhang [7] tried to employ the stress-based criterion to predict the delamination sizes. Their conclusion is that it has clearly little relevance with reality except perhaps for the initial damage in the thinner plates, but only at the onset. On the other hand, impact tests on thermoset and thermoplastic composites [1] have shown that the delamination results from a dynamic fracture process. It seems that a fracture mechanics approach may be more appropriate for characterizing the delamination. This view has been fully verified by Davies and Zhang [7]. Here, we adopted this viewpoint and only focused on the major delamination of the bottom interface.

3.3.1. Failure criterion for delamination

We employ Griffith criterion of strain energy release rate for the delamination propagation. The failure criterion and some presumptions can be expressed as:

1.
$$\begin{cases} G \leq G_C & \text{not extend} \\ G > G_C & \text{extend} \end{cases} \tag{7}$$
where G_C is the value of the critical or threshold strain energy release rate.
2. At a specific moment, the stresses at the front of the delamination are assumed to maintain unchanged while the crack grows.
3. The critical strain energy release rate G_C is assumed to be a constant.
4. The crack grows along the direction in which the largest strain energy release rate is produced.

Here, we use a series of line segments to approximate the profile of the delamination front. For this purpose, a technique for computing the strain energy release rate at the delamination front in the Mindlin plate model is

Table 2
Strategy of updating elastic constants

Updating strategy of stress in Ref. [8]	$\sigma_{11}=\sigma_{22}=\sigma_{33}=0,$ $\sigma_{12}=\sigma_{23}=\sigma_{31}=0$ (fiber failure)	$\sigma_{22}=0,\ \sigma_{12}=0$ (matrix cracking)	$\sigma_{22}=0$ (matrix crushing)
Updating strategy of elastic constant in this paper $d\gg 0$, $e/\min(E_i,v_j,G_k)>0$, $e/\min(E_i,v_j,G_k)\ll 1$	$E_i=\max(E_i/d,e)$ $v_{ij}=\max(v_{ij}/d,e)$ $G_{ij}=\max(G_{ij}/d,e)$ (fiber failure)	$E_2=\max(E_2/d,e)$ $v_{12}=\max(v_{12}/d,e)$ $G_{12}=\max(G_{12}/d,e)$ (matrix cracking)	$E_2=\max(E_2/d,e)$ $v_{12}=\max(v_{12}/d,e)$ (matrix crushing)

Note: $i,j,k=1,2,3$, if not specified.

proposed. Considering two small rectangular elements L and D shown in Fig. 4, which represent intact part and delaminated part respectively, the delamination extension can be thought of as a transition from state L to state D. Firstly, the increment of elastic strain energy during the deformation from L to D is

$$\delta p = \frac{1}{2}\int ({}'\sigma_{ij}{}'e_{ij} + {}'\sigma_{i3}{}'e_{i3} - \sigma_{ij}e_{ij} - \sigma_{i3}e_{i3})\mathrm{d}z, \quad (i,j=1,2) \tag{8}$$

where σ_{ij}, e_{ij}, ${}'\sigma_{ij}$ and ${}'e_{ij}$ represent the in-plane stresses and strains of elements L and D, respectively. Similarly, σ_{i3}, e_{i3}, ${}'\sigma_{i3}$ and ${}'e_{i3}$ represent the transverse shear stresses and strains, of elements L and D, respectively.

Secondly, according to presumption 2 stated above, the work of internal forces during deformation is:

$$\delta w = \int [{}'\sigma_{ij}({}'e_{ij} - e_{ij}) + {}'\sigma_{ie}({}'e_{i3} - e_{i3})]\mathrm{d}z, \quad (i,j=1,2) \tag{9}$$

Then, the energy released can be written as:

$$\delta\pi = \delta w - \delta p \tag{10}$$

Therefore, the strain energy release rate G is:

$$G = \frac{\delta\pi}{\delta A} = \int [{}'\sigma_{ij}({}'e_{ij} - e_{ij}) + {}'\sigma_{ie}({}'e_{i3} - e_{i3}) - \frac{1}{2} \times ({}'\sigma_{ij}{}'e_{ij} + {}'\sigma_{i3}{}'e_{i3} - \sigma_{ij}e_{ij} - \sigma_{i3}e_{i3})]\mathrm{d}z/\delta A, \quad (i,j=1,2) \tag{11}$$

Here, in fact, we utilize a hybrid model by comprehensively considering the effects of the tension and transverse shear stress/strain components. The above theory for calculating the strain energy release rate is similar to that in Ref. [17], but we extended it from the classical plate theory into the Mindlin plate theory.

3.3.2. Modeling delamination and solution of dynamic contact problem

A quarter of the plates in Fig. 1, i.e. the top right corner, is modeled using the FEM mesh as shown in Fig. 5. For 0°/90°/0° cross-ply laminates under the low-velocity impact, the major delamination only appears on the bottom interface, i.e. 90°/0° interface. Without an onset criterion for

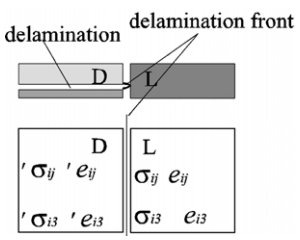

Fig. 4. View of the delamination front for calculating strain energy release rate (upper diagram is front view and lower diagram is top view).

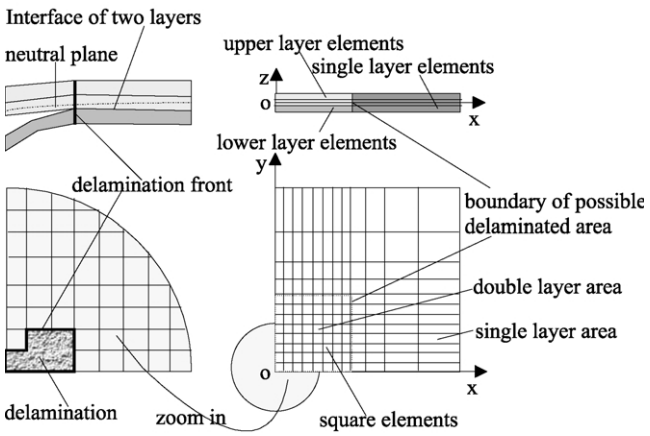

Fig. 5. FEM model.

delamination, we presume that there is an initial tiny delaminated element under the impact point. It was found that the results, e.g. final delamination size, are insensitive to the pre-defined initial delamination size when the area of this element is small enough (less than 0.05% of the whole p late). Furthermore, the portion of plates near the impact p oint, which is considered the possible delaminated area, is meshed into double-layer Mindlin plate elements, while the portion far from the impact point is meshed into single-layer Mindlin plate elements, as shown in Fig. 5. Naturally, the continuity of the displacements on the borderline between the single-layer portion and the double-layer portion should be maintained. Also, before delamination occurs, three displacement components on the interfaces of the upper/lower elements within the double-layer portion are enforced to be identical using the penalty functions. After the occurrence of delamination, these penalty functions should be removed and the contact effect must be taken into account at the interface. Prompted by the idea in Ref. [18], we construct a first-order continuous penalty function, letting

$$p_z = \begin{cases} \bar{p}_z\, \mathrm{e}^{-\beta g_z} & g_z \geq 0, \text{ not impenetrate} \\ \bar{p}_z - k g_z^q & g_z < 0, \text{ impenetrate} \end{cases}, \quad (\beta, k \gg 0) \tag{12}$$

where $g_z = \hat{w}_{up} - \hat{w}_{low}$ is the gap function, and $\bar{p}_z$ is the actual normal contact force.

The above strategy neglects friction between the two delaminated layers. It can be recognized that p_z in Eq. (12) is just the correction term conjugate to the normal contact force between delaminated layers. $\bar{p}_z$ is an unknown quantity, which can be obtained implicitly by using the following iteration scheme:

$$\text{loading stage}: \quad {}^{i+1}p_z = \begin{cases} {}^{i}p_z\, \mathrm{e}^{-\beta(g_z^i + g_z^{i+1})} & {}^{i}g_z \geq 0, \text{ not impenetrate} \\ {}^{i}p_z - k(g_z^i + g_z^{i+1})^q & {}^{i}g_z < 0, \text{ impenetrate} \end{cases} \tag{13a}$$

$$\text{unloading stage}: \quad {}^{i+1}p_z = -k g_z^{i+1} \tag{13b}$$

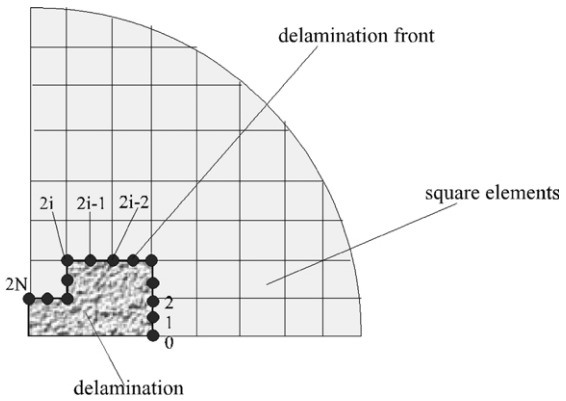

Fig. 6. Schematic view of delamination extension.

It has been identified [4,7,10] that all damages are completed before the maximum impact force. Here, to reduce the computational cost, in the unloading stage, we employed a simple technique, in which, the two delaminated layers are connected to move together by limiting the contact iteration number to be 1 and inserting the strong penalty functions at the interface. The selection of parameter q will directly affect the rate of convergence. We set $q = 1.5$ from numerical experiences.

3.3.3. Implementation of delamination failure criterion

As shown in Fig. 6, assuming that the profile of the delamination front and the neighboring stresses/strains at time t are known, we simulate the delamination extension using the following procedure:

1. Perform stress extrapolation and stress smoothing using the Gaussian integration points on elements on the delamination front.
2. Calculate the strain energy release rate G_i $(i = 0, 1, 2, \ldots, 2N-1, 2N)$, of the points on the delamination front by employing Eq. (11).
3. Calculate the average strain energy release rate of line segments on the delamination front $G^i = (G_{2i-2} + G_{2i-1} + G_{2i})/3$ $(i = 1, 2, \ldots, N)$.
4. Sort G^i and obtain the sequence $G^{i_1} \geq G^{i_2} \geq \cdots G^{i_N} \geq 0$.
5. Under the delamination growth criterion, i.e. Eq. (7) and the presumption 4 in Section 3.3.1, if $G^{i_k} \geq G_C \geq G^{i_{k+1}}$, we let the delamination extend n elements along the exterior normals of the line segments $i_1, i_2, \ldots, i_{k'}$ $(k' \leq k)$, where k' is a parameter and n represents the growth length within one time increment Δt. In the present FEM codes, we keep $k' \equiv 1$ in all our numerical simulations. That means, among all the segments that are greater than G_c, only the one with the largest strain energy release rate extends within one time step. Obviously, it is unreasonable to let all segments of the larger strain energy release rate than the critical one extend simultaneously since the stress/strain fields will be redistributed after the extension of the segment of the largest strain energy release rate. If the actual crack growth length is less than one element length within the time increment Δt, n should be kept as 1. In computation, this requirement is satisfied by automatically adjusting the time increment. Simply speaking, when the calculated energy release rate becomes closer to the critical value, we gradually reduce the current time increment in proportion. Also, as long as the delamination extension occurs, we further reduce the time step in proportion. In this case, it is reasonable to set $n = 1$, i.e. the extension of one element within one time step.
6. Update data structure and form a new profile of the delamination.

3.4. Adaptive strategy

The adaptive strategy includes the following three aspects: (a) adjusting the time increment according to stress rate; (b) updating the stiffness matrix according to the current extent of deformation; (c) modifying penalty parameters according to the current degree of damage, which are explained as follows.

Generally, the time increment should be adjusted according to the damage evolution and the extent of deformation instead of keeping constant. In the FEM code, we take the impact point as the reference point. According to the stress rate at this point, we automatically adjust the time increment under the precondition of sufficient precision.

Because some local areas of laminates are in the state of large deformation during the impact process, the non-linear stiffness matrix needs to be updated step-by-step including its re-formation and re-decomposition. To reduce the computational cost, in the FEM code, we use the deflection at the impact point as a yardstick to measure the extent of deformation of laminates, and then to decide whether to update the stiffness matrix. Specifically, whenever the deflection at impact point accumulatively increases by a fixed constant within some time steps, the stiffness matrix is then updated once. This constant is set from experience to be around 0.3% of the total thickness of plates.

Two penalty parameters in Eqs. (13a) and (13b), β and k, have the direct influence on the convergence property of the contact iteration. We adjust the parameter k according to the equivalent bending stiffness in the delaminated area, which decreases due to the delamination and the updating of material constants caused by the matrix cracks as shown in Table 2. We set k to be the product of the greatest bending stiffness coefficients in the delamination area and a specific large positive value, e.g. 1000.0. Furthermore, we adjust parameter β according to the current average delamination gap. Practically β can be set to be the product of the average gap and an adjustment factor, which is determined by the approach of trial and error. This adjustment factor is chosen to be 1.5 to attain a satisfactory convergence rate.

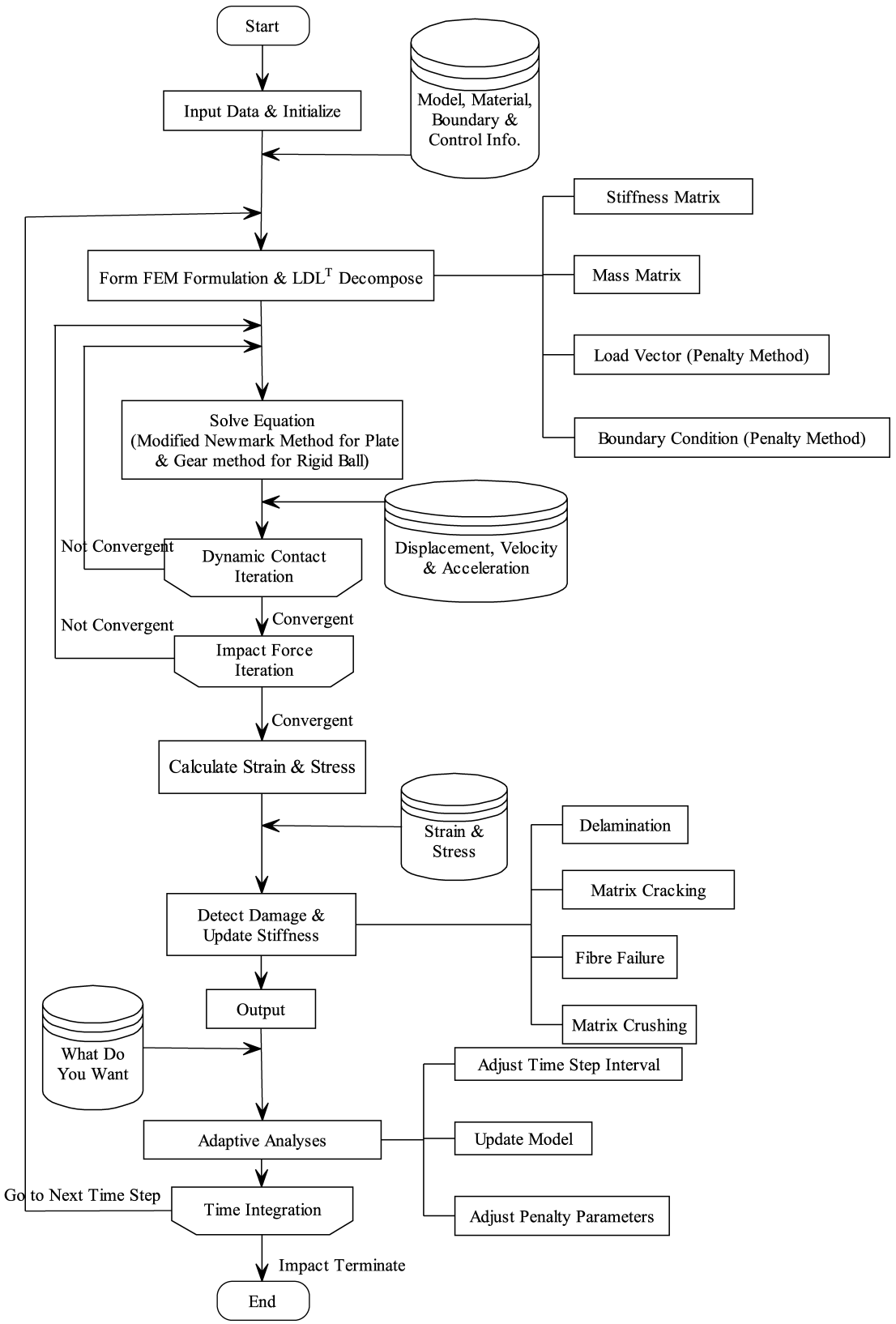

Fig. 7. Flowchart of FEM program.

4. Flow chart of the present FEM code

Based on the previous proposed numerical model, we developed an FEM code, which is shown in Fig. 7. There are three major loops in this flowchart. The outermost loop is the time integration loop for computing the responses at the various time points. Before the step obtaining the strain/stress, there are two non-linear iteration loops. The outer loop is the non-linear iteration for solving the impact force calculated by Eq. (3). The inner loop is the non-linear iteration for analyzing the dynamic contact problems between the delaminated layers using Eqs. (13a) and (13b). Both non-linear iterations are carried out using the Newton–Raphson algorithm.

5. Conclusions

We have developed an FEM model based on the 9-node Mindlin plate element for directly simulating the low-velocity impact-induced damage in laminated plates. This is an integrated numerical model, which includes various aspects, such as the damage criteria for the various damages, the updating strategy of plates stiffness due to various damages, the efficient solution of the ordinary differential equation of the rigid ball, the detailed modeling of the various damages, the dynamic contact problem between delaminated layers, adaptive techniques for enhancing the computational efficiency, etc. In fact, this complicated and detailed numerical model has been set up based on our long-term work in this field from 1995. Many critical aspects of this code based on the proposed approach have been verified through many previous experimental and numerical results [11–13,17]. In Part II of this two part series, we will further demonstrate the justification and effectiveness of the present approach through the comparison with some experimental results. After the verification, many aspects of the low-velocity impact-induced damage process will also be investigated through the solution of many carefully designed models using the present numerical technique.

Acknowledgements

We would like to thank Professor W.M. Zheng for his help. Computer systems used include the 144-node TS108 cluster system at Tsinghua University, and SW I system at Beijing High Performance Computer Center. Some authors were supported by the Natural Science Foundation of China under Grant 59875045 and by Basic Research Foundation of Tsinghua University under Grant JC200020.

References

[1] Sun CT, Grady JE. Dynamic delamination fracture toughness of a graphite/epoxy laminate under impact. Compos Sci Technol 1988;31:55–72.
[2] Choi HY, Wu HY, Chang FK. A new approach toward understanding damage mechanisms and mechanics of laminated composites due to low-velocity impact. Part II. Analysis. J Compos Mater 1991;25:1012–38.
[3] Choi HY, Wu HY, Chang FK. Effect of laminate configuration and impactor's mass on the initial impact damage of graphite/epoxy composite plates due to line-loading impact. J Compos Mater 1992;26:804–27.
[4] Choi HY, Chang FK. A model for predicting damage in graphite/epoxy laminated composites resulting from low-velocity point impact. J Compos Mater 1992;26:2134–69.
[5] Collombet F, Lalbin X, Lataillade JL. Impact behavior of laminated composites: physical basis finite element analysis. Compos Sci Technol 1998;58:463–78.
[6] Hou JP, Petrinic N, Ruiz C, Hallett SR. Prediction of impact damage in composite plates. Compos Sci Technol 2000;60:273–81.
[7] Davies GAO, Zhang X. Impact damage prediction in carbon composite structures. Int J Impact Engng 1995;16:149–70.
[8] Zheng S, Sun CT. A double-plate finite element model for the impact-induced delamination problem. Compos Sci Technol 1995;53:111–8.
[9] Davies GAO, Hitchings D, Wang J. Prediction of threshold impact energy for onset of delamination in quasi-isotropic carbon/epoxy composite laminates under low-velocity impact. Compos Sci Technol 2000;60:1–7.
[10] Wang H, Vu-Khanh T. Fracture mechanics and mechanisms of impact-induced delamination in laminated composites. J Compos Mater 1995;29:156–78.
[11] Hu N. A solution method for dynamic contact problems. Comput Struct 1997;63:1053–63.
[12] Sekine H, Hu N, Natsume T, Fukunaga H. Low-velocity impact response analysis of composite laminate with a delamination. Mech Compos Mater Struct 1998;5:257–78.
[13] Hu N, Sekine H, Fukunaga H, Yao ZH. Impact analysis of composite laminates with multiple delaminations. Int J Impact Engng 1999;22:633–48.
[14] Pica RDW, Hinton E. Finite element analysis of geometrically non-linear plate behavior using a Mindlin formulation. Comput Struct 1980;11:203–15.
[15] Tan TM, Sun CT. Wave propagation in graphite/epoxy laminates due to impact. J Appl Mech 1985;52:6–12.
[16] William HP. Numerical recipes in C: the art of scientific computing, 2nd ed. Cambridge: Syndicate; 1995. p. 734–48.
[17] Kamiya S, Sekine H, Yagishita Y. Computational simulation of interlaminar crack extension in angle-ply laminates due to transverse loading. J Compos Mater 1998;32:744–65.
[18] Zavarise G, Wriggers P, Schrefler BA. A method for solving contact problems. Int J Numer Meth Engng 1998;42:473–98.